

1 **Hydroclimatic variability in the southwestern Indian Ocean between 6000 and 3000 years ago**

2  
3 Hanying Li<sup>1</sup>, Hai Cheng<sup>1, 2\*</sup>, Ashish Sinha<sup>3</sup>, Gayatri Kathayat<sup>1</sup>, Christoph Spötl<sup>4</sup>, Aurèle Anquetil  
4 André<sup>5</sup>, Arnaud Meunier<sup>5</sup>, Jayant Biswas<sup>6</sup>, Pengzhen Duan<sup>1</sup>, Youfeng Ning<sup>1</sup>, R. Lawrence Edwards<sup>2</sup>

5  
6 <sup>1</sup>Institute of Global Environmental Change, Xi'an Jiaotong University, China

7 <sup>2</sup>Department of Earth Sciences, University of Minnesota, Minneapolis, USA

8 <sup>3</sup>Department of Earth Science, California State University Dominguez Hills, Carson, USA

9 <sup>4</sup>Institute of Geology, University of Innsbruck, Innsbruck, Austria

10 <sup>5</sup>Francois Leguat Giant Tortoise and Cave Reserve, Anse Quito, Rodrigues Island, Mauritius

11 <sup>6</sup>National Cave Research and Protection Organization, Raipur, India

12  
13  
14 \*Correspondence and requests for materials should be addressed to H.C. (email: cheng021@xjtu.edu.cn)

15  
16 **Abstract**

17 **The ‘4.2 ka event’ is frequently described as a major global climate anomaly between 4.2**  
18 **and 3.9 ka BP, which defines the beginning of the current Meghalayan age in the Holocene epoch.**  
19 **The ‘event’ has been disproportionately reported from proxy records from Northern Hemisphere**  
20 **but its climatic manifestation remains much less clear in Southern Hemisphere. Here, we present**  
21 **highly resolved and chronologically well-constrained speleothem oxygen and carbon isotopes**  
22 **records between ~6 and 3 ka BP from Rodrigues Island in the southwestern subtropical Indian**  
23 **Ocean, located ~600 km east of Mauritius. Our records show that the ‘4.2 ka event’ did not**  
24 **manifest as a period of major climate change at Rodrigues Island in the context of our record’s**  
25 **length. Instead, we find evidence for a multi-centennial drought that occurred near-continuously**  
26 **between 3.9 and 3.5 ka BP and temporally coincided with climate change throughout the**  
27 **Southern Hemisphere.**

## 40 **1. Introduction**

41 The '4.2 ka event' is considered as a widespread climate event between 4.2 and 3.9 ka BP  
42 (thousand years before present, where present = 1950 AD) (e.g., Weiss et al., 1993, 2016). Many  
43 paleoclimate records from the Northern Hemisphere (NH) have characterized the event as a multi-  
44 decadal to multi-centennial period of arid and cooler conditions across the Mediterranean, Middle East,  
45 South Asia and North Africa (e.g., Finné et al., 2011; Marchant and Hooghiemstra, 2004; Migowski et  
46 al., 2006; Mayewski et al., 2004; Staubwasser et al., 2003; Arz et al., 2006; Zielhofer et al., 2017;  
47 Stanley et al., 2003; Kathayat et al., 2017). The structure of the '4.2 ka event' from many proxy records  
48 such as peat cellulose records from the eastern Tibetan Plateau (Hong et al., 2003, 2018), speleothem  
49 from northeastern India (Berkelhammer et al., 2012) and southern Italy (Drysdale et al., 2006), marine  
50 sediments from the Gulf of Oman (Cullen et al., 2000) and the northern Red Sea (Arz et al., 2006), and  
51 the dust record in the Kilimanjaro ice core (Thompson et al., 2002) typically characterized it as a single  
52 pulse-like signal in the long term context of these records. In contrast, the structure of '4.2 ka event' in  
53 Southern Hemisphere (SH) remains unclear. Some proxy records from the tropical and sub-tropical  
54 regions of Africa and Australia show a shift towards drier conditions around 4 ka BP (e.g., Russell et  
55 al., 2003; Marchant and Hooghiemstra, 2004; Griffiths et al., 2009; Denniston et al., 2013; Berke et al.,  
56 2012; De Boer et al., 2013, 2014, 2015; Schefuß et al., 2011; Rijdsdijk et al., 2009, 2011). Other records  
57 show virtually unchanged hydrological conditions (e.g., Tierney et al., 2008, 2011; Konecky et al.,  
58 2011) or a two-pulsed multi-decadal length wet events (Railsback et al., 2018) during the period  
59 contemporaneous with the 4.2 ka event.

60 The goal of this study is to investigate a time period that spans the '4.2 ka event' in a key region  
61 of the SH via highly resolved and precisely dated proxy records. Here, we present speleothem oxygen  
62 ( $\delta^{18}\text{O}$ ) and carbon ( $\delta^{13}\text{C}$ ) isotope records from La Vierge (LAVI-4) and Patate (PATA-1) caves from the  
63 Rodrigues Island (Fig.1) in the southern subtropical Indian Ocean. The LAVI-4 and PATA-1 records  
64 span from ~6 to 3 ka BP and from ~6.1 to 3.3 ka BP, with an average resolution of ~4 and 14 years,  
65 respectively. The LAVI-4, which constitutes our primary record, has a precise age control and a sub-  
66 decadal resolution, which, together with PATA-1 record, allows us to reliably characterize the multi-  
67 decadal to centennial hydroclimate variations in the southwestern Indian Ocean during the period from  
68 6 to 3 ka BP.

## 69 **2 Modern climatology**

### 70 **2.1 Climatology**

71 Rodrigues (~19°42'S, ~63°24'E) is a small volcanic island (~120 km<sup>2</sup>) situated in the  
72 southwestern Indian Ocean, ~600 km east of Mauritius (Fig. 1). The island's maximum altitude is ~400  
73 m above sea level. Rodrigues' mean annual temperature is ~24°C and the mean annual rainfall is ~1010  
74 mm, of which nearly 70% occurs during the wet season (November to April) with February being the  
75 wettest month. The seasonal distribution of rainfall is largely controlled by the seasonal migration of the  
76 ITCZ and the Mascarene High (Senapathi et al., 2010; Rijdsdijk et al., 2011; Morioka et al., 2015) (Fig.  
77 1). Given its location at the southern fringe of the ITCZ, the austral summer rainfall at Rodrigues is very  
78 sensitive to the mean position of the southern limit of the ITCZ. This is highlighted by backward (120  
79 hours) HYSPLIT (Draxler and Hess, 1998) trajectory composites of the low-level winds (850 hPa)  
80 during the years when the total January to March (JFM) precipitation was unusually low (dry) and high  
81 (wet) than the long-term mean (1951-2016) at Rodrigues (Fig. 1B). Of note is a major increase in the  
82 fraction of air parcel trajectories arriving from the north of Rodrigues during the wetter years, indicating  
83 an enhanced contribution of northerly moisture resulting from a more southerly position of the ITCZ

84 (Fig. 1B). This observation is further supported by analyses of the low-level wind trajectory cluster  
85 composites of February in those years when the southern boundary of the the ITCZ was anomalously  
86 north or south (Lashkari et al., 2017; Freitas et al., 2017) of its long-term mean February position  
87 (Supplementary Fig. 1 A-B). In addition to the ITCZ, ENSO also modulates austral summer  
88 precipitation at Rodrigues via modulating the Hadley and Walker circulations (Senapathi et al., 2010; De  
89 Boer et al., 2014; Griffiths et al., 2016; Zinke et al., 2016). Instrumental data and our trajectory  
90 composites for selected El Niño and La Niña years suggest that an increased (decreased) summer  
91 precipitation at Rodrigues is associated with the El Niño (La Niña) events (Supplementary Fig. 1C-D).

## 92 **2.2 Oxygen isotopes and climatology**

93 Modern observations of  $\delta^{18}\text{O}$  of precipitation ( $\delta^{18}\text{O}_p$ ) in the study area are unavailable due to the  
94 lack of Global Network of Isotopes in Precipitation (GNIP) stations in Rodrigues. However,  $\delta^{18}\text{O}_p$  data  
95 from the nearest GNIP station in Mauritius show a clear annual cycle in  $\delta^{18}\text{O}_p$  with depleted values  
96 during the austral summer (Supplementary Fig. 2A). Additionally, in the absence of GNIP data, we use  
97 simulated  $\delta^{18}\text{O}_p$  data from the Experimental Climate Prediction Center's Isotope-incorporated Global  
98 Spectral Model (IsoGSM) (Yoshimura et al., 2008) to assess the large-scale dynamical processes that  
99 control  $\delta^{18}\text{O}_p$  on interannual and decadal timescales. Our analyses show the presence of a strong  
100 negative correlation between the  $\delta^{18}\text{O}_p$  and rainfall amount similar to the 'amount effect' (e.g.,  
101 Dansgaard, 1964) (Supplementary Fig. 2B-C). We therefore interpret  $\delta^{18}\text{O}_p$  variations in the cave  
102 catchment and, consequently, in speleothems from this region primarily reflecting variations in rainfall  
103 amount in response to both local and large-scale atmospheric circulation changes. The relationship is  
104 such that more negative (positive)  $\delta^{18}\text{O}_p$  values occur during times of either an anomalously southward  
105 (northward) position of the southern boundary of the ITCZ or El Niño (La Niña) conditions.

## 106 **3 Methods**

### 107 **3.1 Speleothem samples**

108 Two stalagmites, LAVI-4 and PATA-1, from La Vierge and Patate caves, respectively, were used  
109 in this study. La Vierge (19°45'26"S, 63°22'13"E, ~32 m asl) and Patate (19°45'30"S, 63°23'11"E, ~20  
110 m asl) caves are located in Plaine Corail and Plaine Caverne, respectively, in southwestern Rodrigues  
111 (Middleton and David, 2013). The cave temperature and relative humidity at the time of sample  
112 collection (June 2015) were ~25.5°C and 95% in La Vierge cave and ~22.5°C and 95% in Patate cave.  
113 Samples LAVI-4 and PATA-1 were collected at the distance of ~50 m and 200 m from cave entrances,  
114 respectively. The diameters of LAVI-4 and PATA-1 are ~75 and 95 mm, and their lengths are ~400 and  
115 ~334 mm, respectively. Both stalagmites were cut along their growth axes using a thin diamond blade  
116 and then polished.

### 117 **3.2 $^{230}\text{Th}$ dating**

118 Subsamples (80-130 mg) for  $^{230}\text{Th}$  dating were drilled using a 0.9 mm carbide dental drill.  $^{230}\text{Th}$   
119 dating was performed at Xi'an Jiaotong University, China, by using a Thermo-Finnigan Neptune *plus*  
120 multi-collector inductively coupled plasma mass spectrometer (MC-ICP-MS). The method is described  
121 in Cheng et al. (2000, 2013). We used standard chemistry procedures (Edwards et al., 1987) to separate  
122 U and Th. A triple-spike ( $^{229}\text{Th}$ - $^{233}\text{U}$ - $^{236}\text{U}$ ) isotope dilution method was used to correct instrumental  
123 fractionation and to determine U/Th isotopic ratios and concentrations (Cheng et al., 2000, 2013). U and  
124 Th isotopes were measured on a MasCom multiplier behind the retarding potential quadrupole in the  
125 peak-jumping mode using standard procedures (Cheng et al., 2000). Uncertainties in U and Th isotopic  
126 measurements were calculated offline at the  $2\sigma$  level, including corrections for blanks, multiplier dark

127 noise, abundance sensitivity, and contents of the same nuclides in the spike solution.  $^{234}\text{U}$  and  $^{230}\text{Th}$   
128 decay constants of Cheng et al. (2013) were used. Corrected  $^{230}\text{Th}$  ages assume an initial  $^{230}\text{Th}/^{232}\text{Th}$   
129 atomic ratio of  $(4.4 \pm 2.2) \times 10^{-6}$ , and the value for material at secular equilibrium with the bulk earth  
130  $^{232}\text{Th}/^{238}\text{U}$  value of 3.8. The correction for a few samples LAVI-4 and PATA-1 are large, because either  
131 U concentration is low ( $\sim 65$  ppb) and/or the detrital  $^{232}\text{Th}$  concentration is elevated ( $>100$  ppt) (Table  
132 S1, Fig. 2).

### 133 **3.3 Stable isotope analysis**

134 LAVI-4 and PATA-1 stable isotope ( $\delta^{18}\text{O}$  and  $\delta^{13}\text{C}$ ) records were established by  $\sim 962$  and  $\sim 190$   
135 data, respectively. The New Wave Micromill, a digitally controlled tri-axial micromill equipment, was  
136 used to obtain subsamples. The subsamples ( $\sim 80$   $\mu\text{g}$ ) were continuously micromilled along the  
137 stalagmites growth axes of LAVI-4 and PATA-1 at increments between 100 and 200  $\mu\text{m}$ . The  
138 subsamples of LAVI-4 were measured using a Finnigan MAT-253 mass spectrometer coupled with an  
139 on-line carbonate preparation system (Kiel-IV) in the Isotope Laboratory, Xi'an Jiaotong University.  
140 The subsamples of PATA-1 were measured using an on-line carbonate preparation system (GasbenchII)  
141 connected to an isotope ratio mass spectrometer (Delta<sup>plus</sup>XL) in the Isotope Laboratory, Innsbruck  
142 University. The latter technique is reported in Spötl (2011) and Spötl and Vennemann (2003). All  
143 results are reported in per mil (‰) relative to the Vienna PeeDee Belemnite (VPDB) standard.  
144 Duplicate measurements of standards show a long-term reproducibility of  $\sim 0.1\%$  ( $1\sigma$ ) or better (Table  
145 S2, Fig. 2).

## 146 **4 Results**

### 147 **4.1 Age models**

148 We obtained 26 and 7  $^{230}\text{Th}$  dates for samples LAVI-4 and PATA-1, respectively. The LAVI-4  
149 and PATA-1 age models and associated uncertainties were constructed using COPRA (Constructing  
150 Proxy Records from Age) (Breitenbach et al., 2012) and ISCAM (Intra-Site Correlation Age Modelling)  
151 (Fohlmeister, 2012) age modelling schemes (Supplementary Fig. 3). Both schemes yielded virtually  
152 identical age models, and thus the conclusions of this study are not sensitive to the choice of the age  
153 model (Fig. 2 and Supplementary Fig. 3).

154 The time interval from 6 to 3 ka BP in LAVI-4 speleothem corresponds to a sample depth of 274  
155 to 81 mm below the top, respectively. A drip-water relocation occurred at a depth of 124 mm, which is  
156 associated with a Type L surface characterized by slow growth and narrow layers under progressively  
157 drier conditions (Railsback et al., 2013) (Supplementary Figs. 3 and 4). It cannot be ruled out that there  
158 also exists a hiatus at this depth ( $\sim 3.5$  ka BP). If such a hiatus was indeed present, its duration would be  
159 about 100 years based on the age model (Supplementary Fig. 4). The time interval from 6.1 to 3.3 ka BP  
160 in PATA-1 corresponds to a sample depth of 34 to 15 mm. Growth of PATA-1 ceased at  $\sim 15$  mm and  
161 then resumed about 630 years later, creating a hiatus (Supplementary Fig. 3). The COPRA age models  
162 of PATA-1 and LAVI-4 (Fig. 2 and Supplementary Fig. 3) are reported in Table S2 and used in the  
163 following discussion.

### 164 **4.2 Isotopic equilibrium tests**

165 Conventional criteria to assess isotopic equilibrium of stalagmites are provided by the Hendy Test  
166 (Hendy, 1971), which requires no correlation between  $\delta^{18}\text{O}$  and  $\delta^{13}\text{C}$  values measured along the growth  
167 axis as well as along the same growth lamina. The correlation between the  $\delta^{18}\text{O}$  and  $\delta^{13}\text{C}$  values in  
168 LAVI-4 and PATA-1 is 0.53 and 0.85, respectively, which suggests the possibility of isotopic  
169 disequilibrium during calcite precipitation. However, a number of studies (e.g., Dorale and Liu, 2009)  
170 pointed out that a correlation between  $\delta^{18}\text{O}$  and  $\delta^{13}\text{C}$  values does not automatically rule out isotopic

171 equilibrium. Instead, the replication test (i.e., a high degree of coherence between  $\delta^{18}\text{O}$  profiles of  
172 individual speleothems from the same cave) is a more rigorous and reliable test of isotopic equilibrium.  
173 Particularly, the replication test is far more robust if the records used are from different caves with  
174 different kinetic/vadose-zone processes, such is the case for this study. Indeed, a high degree of visual  
175 similarity between the coeval portions of LAVI-4 and PATA-1  $\delta^{18}\text{O}$  and  $\delta^{13}\text{C}$  records suggest that both  
176 stalagmites record primary climate signals, notwithstanding the offsets between the absolute values (Fig.  
177 2A). The replication is further confirmed by statistically significant correlations between the LAVI-4  
178 and PATA-1  $\delta^{18}\text{O}$  ( $r=0.64$  at 95% confidence level) and  $\delta^{13}\text{C}$  ( $r=0.73$  at 95% confidence level) records  
179 calculated using the ISCAM algorithm (Fohlmeister, 2012) for their contemporary growth period  
180 between 3.4 and 6.0 ka BP (Fig. 2). ISCAM uses a Monte Carlo approach to find the best correlation  
181 between the proxy records by adjusting each record within its dating uncertainty. The significant levels  
182 are assessed against a red-noise background generated using artificially simulated first-order  
183 autoregressive time series (AR1). The offset in absolute  $\delta^{18}\text{O}$  values between LAVI-4 and PATA-1,  
184 however, remains unclear, and possibly arises from processes related to the characteristics of the two  
185 karst systems, such as temperature differences as observed during our fieldwork in 2015. Therefore, in  
186 the following discussion we focus only on temporal variations of LAVI-4  $\delta^{18}\text{O}$  and  $\delta^{13}\text{C}$  records due to  
187 their higher resolution and better constrained chronology (Fig. 2).

## 188 **5 Discussion and Conclusions**

### 189 **5.1 Proxy interpretation**

190 The temporal resolution of the LAVI-4  $\delta^{18}\text{O}$  record between 6 and 3 ka BP varies from 1.2 to 16.4  
191 years with an average resolution of  $\sim 3.2$  years. The  $\delta^{18}\text{O}$  temporal variability is large ( $\sim 3.5$  ‰) and, as  
192 noted earlier, we interpret the  $\delta^{18}\text{O}$  variations to dominantly reflect changes in the precipitation amount.  
193 This line of reasoning is justified given the island's isolated setting far removed from large-sized  
194 landmasses and its low topographic relief, which minimizes isotopic variability stemming from  
195 processes such as the continentality and altitude effects as well as mixing of distant water vapor sources  
196 with significantly different isotopic compositions. This interpretation is additionally supported by  
197 moderate to strong covariance between the LAVI-4  $\delta^{18}\text{O}$  and  $\delta^{13}\text{C}$  profiles. Although the process of  
198 stalagmite precipitation may be affected by evaporation and/or degassing (Treble et al., 2017; Cuthbert  
199 et al., 2014; Markowska et al., 2016; McDermott, 2004; Lachniet, 2009), the temporal variations in the  
200 latter can stem from changes in vegetation type and density, soil microbial productivity, prior calcite  
201 precipitation (PCP) and groundwater infiltration rates (e.g., Baker et al., 1997; Genty et al., 2003), all of  
202 which may drive  $\delta^{18}\text{O}$  and  $\delta^{13}\text{C}$  values in the same fashion (e.g., Brook et al., 1990; Dorale et al., 1992;  
203 Bar-Matthews et al., 1997). The significant covariance between the  $\delta^{13}\text{C}$  and  $\delta^{18}\text{O}$  records could  
204 therefore, indicate that both proxies reflect a common response to changes in rainfall amount at  
205 Rodrigues, or a rainfall limit on the extent of vegetation and other related processes in the epikarst as  
206 mentioned above.

### 207 **5.2 Hydroclimate variability between 6 and 3 ka BP at Rodrigues**

208 The z-score transformed profiles of LAVI-4  $\delta^{18}\text{O}$  and  $\delta^{13}\text{C}$  records reveal several decadal to  
209 multi-decadal intervals of significantly drier and wetter conditions ( $> \pm 1$  standard deviation) (Fig. 3) but  
210 no distinct long-term trends (Figs. 2 and 3). The interval corresponding to the '4.2 ka event' in the  
211 LAVI-4  $\delta^{18}\text{O}$  record, typically between 4.2 and 3.9 ka BP (e.g., Weiss et al., 2016), includes two dry  
212 ( $\sim 4200$  to 4130 yr. BP and  $\sim 4020$  to 3975 yr. BP) and two wet ( $\sim 4130$  to 4020 yr. BP and  $\sim 3975$  to  
213 3945 yr. BP) periods (Fig. 3). During this time interval the LAVI-4  $\delta^{13}\text{C}$  record shows two wet periods  
214 peaking at  $\sim 4115$  and 4015 yr BP, respectively, which correlate within age uncertainties with two wet

215 pulses in proxy records from Mawmluh cave (Kathayat et al., 2018), Tangga cave (Wurtzel et al., 2018),  
216 Makassar Strait (Tierney et al., 2012), Liang Luar cave (Griffiths et al., 2009), KNI-51 cave (Denniston  
217 et al., 2013) and Dante cave (Railsback et al., 2018) (Fig. 4).

218 Overall, the climate variations recorded at Rodrigues from 4.2 to 3.9 ka BP are characterized by  
219 high-frequency (decadal to multi-decadal) fluctuations, including the major arid/wet events mentioned  
220 above. Notably, however, the mean hydroclimatic state of this time interval inferred from both  $\delta^{18}\text{O}$  and  
221  $\delta^{13}\text{C}$  data is indistinguishable from the average state between 6 and 4.2 ka BP (Fig. 3). In this regard,  
222 the climatic events or anomalies between 4.2 and 3.9 ka BP are not distinctly larger in amplitude nor  
223 longer in duration in comparison to similar anomalies between 6 and 4.2 ka BP (Figs. 3 and 4).  
224 Consistently, in the context of the long-term climate variance between 6 and 3 ka BP, there is no  
225 evidence for an unusual climate anomaly between 4.2 and 3.9 ka BP.

226 The most prominent feature of our record is a switch from an interval characterized by high-  
227 frequency  $\delta^{18}\text{O}$  variance (i.e., from 6 to 3.9 ka BP) to a multi-centennial excursion with progressively  
228 higher  $\delta^{18}\text{O}$  and  $\delta^{13}\text{C}$  values: a prolonged megadrought at Rodrigues. Starting at  $\sim 3.9$  ka BP, this  
229 megadrought became progressively more severe leading to a diminished growth rate or a  $\sim 100$  yr-long  
230 hiatus around 3.5 ka BP in LAVI-4. Growth rate picked up subsequently, followed by abrupt ( $\sim 100$  yr-  
231 long) and large decreases in both  $\delta^{18}\text{O}$  ( $\sim 2\%$ ) and  $\delta^{13}\text{C}$  ( $\sim 5\%$ ) to their average values of the entire  
232 records between 6 and 3 ka BP. As such, the structure of the megadrought event shows a saw-tooth  
233 pattern with a multi-centennial drying trend followed by a  $\sim 100$  yr long return to the mean state (Fig. 3).  
234 The multi-century megadrought recorded by our stalagmites between 3.9 and 3.5 ka BP is also evident  
235 in Sahiya cave, north India (Kathayat et al., 2017), and from Lake Edward (Russell et al., 2003), Lake  
236 Victoria (Berke et al., 2012), the Zambezi delta (Schefuß et al., 2011) and the Tatos basin (De Boer et  
237 al., 2014) (Fig. 5). In the eastern sector of the southern Indian Ocean, speleothem records from Tangga  
238 (Wurtzel et al., 2018), KNI-51 (Denniston et al., 2013), and Liang Luar (Griffiths et al., 2009) caves  
239 also show a shift to drier condition at approximately 4 ka BP (Fig. 4).

240 The LAVI-4  $\delta^{13}\text{C}$  record shows a pattern broadly similar to the  $\delta^{18}\text{O}$  record and clearly delineates  
241 three major droughts between 6 and 3 ka BP, centered at 5.43, 4.62 and 3.54 ka BP respectively. These  
242 three drought events share a distinct saw-tooth pattern characterized by a long-term gradual positive  
243 excursion (drying) followed by an abrupt return to the mean values (Fig. 3).

244 To sum, our Rodrigues records show evidence of multidecadal-decadal hydroclimate fluctuations  
245 around the mean state between 6 and 3 ka BP. After 3.9 ka BP, the hydroclimate was characterized by a  
246 multi-centennial trend toward much drier conditions, which ended with a return at  $\sim 3.5$  ka BP within  
247  $\sim 100$  years to the mean hydroclimate state. This pattern is different from the ‘pulse-like’ event between  
248 4.2 and 3.9 ka BP as documented in many other proxy records mainly from the NH. Additionally, the  
249 megadrought between 3.9 and 3.5 ka BP is clearly a later event unrelated to the 4.2 ka event.

### 250 **5.3 Possible mechanisms**

251 A close examination of our Rodrigues  $\delta^{18}\text{O}$  and  $\delta^{13}\text{C}$  records shows that a persistent multi-  
252 centennial drying trend began effectively at  $\sim 4.1$  ka BP and ended at  $\sim 3.5$  ka BP, suggesting a  
253 prolonged northward shift of the mean position of the ITCZ (Fig. 3 and Supplementary Fig. 1A). This  
254 inference, if correct, is partially in contrast with the southward shift of the ITCZ, which is often invoked  
255 to explain the weakening of the Asian monsoon since  $\sim 4.2$  ka BP (e.g., Wang et al., 2005; Kathayat et  
256 al., 2017). Thus, the observed drying trends on both the northern and southern fringes of the ITCZ in  
257 both hemispheres argue against the model of a southward shift in the mean position of the ITCZ as a  
258 viable cause of the 4.2 ka event. A more likely explanation involves an overall contraction in the north-

259 south range of the migrating ITCZ belt in the region (e.g., Yan et al., 2015; Denniston et al., 2016;  
260 Scroxtion et al., 2017). This mechanism is broadly consistent with the spatial pattern of hydroclimate  
261 changes observed in both hemispheres around and after the 4.2 ka event. As mentioned above, the wet  
262 period between ~4.1 and 4.0 ka BP recorded at the northern fringe of the ITCZ (Kathayat et al., 2017;  
263 2018) coincided with a wet period on southern limit of the ITCZ as recorded in Dante cave (Railsback  
264 et al., 2018), the Zambezi Delta (Schefuß et al., 2011), Tatos Basin (De Boer et al., 2014), La Vierge  
265 cave (this study) and KNI-51 cave (Denniston et al., 2013) (Figs. 4 and 5). The subsequent arid period  
266 between ~3.9 and 3.5 ka BP was also basinwide and affected both the northern and southern limits of  
267 the ITCZ over the Indian Ocean and adjacent regions (Figs. 4 and 5).

268 In parallel with drier condition along the southern limit of the austral summer ITCZ, proxy  
269 records from Lake Edward (Russell et al., 2003), Lake Victoria (Berke et al., 2012) and Tangga cave  
270 (Wurtzel et al., 2018), which are located near the northern limit of the contemporary austral summer  
271 ITCZ, also exhibit drier conditions. In contrast, records within the core location of the austral summer  
272 ITCZ, such as Lake Challa (Tierney et al., 2011), Lake Tanganyika (Tierney et al., 2008), Lake Malawi  
273 (Konecky et al., 2011) and Makassar Strait (Tierney et al., 2012), show either slightly wetter or virtually  
274 unchanged hydroclimatic conditions (Figs. 4 and 5). Based on the observed spatial patterns, we suggest  
275 that the contraction of the ITCZ both in terms of a north-south meridional shift as well as with respect to  
276 its overall width may have played an important role in modulating the hydroclimate in our study area  
277 during and after the 4.2 ka event.

## 278 **6 Author Contributions**

279 H.C., A.S. and H.Y.L designed the research and experiments; H.C., A.S., J.B., Y.F.N., A.A.A.,  
280 A.M. and H.Y.L. completed the fieldwork; H.Y.L., H.C., Y.F.N. and C.S. performed stable isotope  
281 measurements and <sup>230</sup>Th dating work. A.S. and H.Y.L. did the data analyses. H.C., H.Y.L. and A.S.  
282 wrote the manuscript, with the help of all co-authors.

## 283 **7 Competing interests**

284 The authors declare no competing financial interests.

## 285 **8 Acknowledgments**

286 We thank Dr. Nick Scroxtion and another anonymous reviewer for their contribution to the peer  
287 review of this work. We very much appreciate editorial helps from Dr. Raymond Bradley. This work  
288 was supported by grants from NSFC (41472140, 41731174 and 41561144003); US NSF grant 1702816;  
289 and a grant from State Key Laboratory of Loess and Quaternary Geology, Institute of Earth  
290 Environment, CAS (SKLLQG1414).

## 291 **9 Data and materials availability**

292 All data needed to evaluate the conclusions in the paper are presented in the paper. Additional  
293 data related to this paper may be requested from the authors. The data will be archived at the National  
294 Climate Data Center (<https://www.ncdc.noaa.gov/data-access/paleoclimatology-data>). Correspondence  
295 and requests for materials should be addressed to H.C. (cheng021@xjtu.edu.cn).

## 296 **References:**

- 297 Arz, H.W., Lamy, F., and Pätzold, J.: A pronounced dry event recorded around 4.2 ka in brine sediments from the northern  
298 Red Sea, *Quaternary Research*, 66, 432–441, 2006.
- 299 Baker, A., Ito, E., Smart, P. L., and McEwan, R. F.: Elevated and variable values of  $^{13}\text{C}$  in speleothems in a British cave  
300 system, *Chemical Geology*, 136, 263-270, 1997.
- 301 Bar-Matthews, M., Ayalon, A., and Kaufman, A.: Late Quaternary paleoclimate in the eastern Mediterranean region from  
302 stable isotope analysis of speleothems at Soreq Cave, Israel, *Quaternary Research*, 47, 155-168, 1997.
- 303 Berke, M. A., Johnson, T. C., Werne, J. P., Grice, K., Schouten, S., and Damsté, J. S. S.: Molecular records of climate  
304 variability and vegetation response since the Late Pleistocene in the Lake Victoria basin, East Africa, *Quaternary  
305 Science Reviews*, 55, 59-74, 2012.
- 306 Berkelhammer, M., Sinha, A., Stott, L., Cheng, H., Pausata, F. S. R., and Yoshimura, K.: An abrupt shift in the Indian  
307 monsoon 4000 years ago, *Geophysical Monograph Series*, 198, 2012.
- 308 Breitenbach, S.F.M., Rehfeld, K., Goswami, B., Baldini, J.U.L., Ridley, H.E., Kennett, D.J., Prufer, K.M., Aquino, V.V.,  
309 Asmerom, Y., Polyak, V.J., Cheng, H., Kurths, J., and Marwan, N.: Constructing Proxy Records from Age models  
310 (COPRA), *Climate of the Past*, 8, 1765–1779, 2012.
- 311 Brook, G. A., Burney, D. A., and Cowart, J. B.: Desert paleoenvironmental data from cave speleothems with examples from  
312 the Chihuahuan, Somali-Chalbi, and Kalahari deserts, *Palaeogeography, Palaeoclimatology, Palaeoecology*, 76,  
313 311-329, 1990.
- 314 Cheng, H., Edwards, R., Hoff, J., Gallup, C., Richards, D., and Asmerom, Y.: The half-lives of uranium-234 and thorium-  
315 230, *Chemical Geology*, 169, 17–33, 2000.
- 316 Cheng, H., Edwards, R.L., Shen, C.-C., Polyak, V.J., Asmerom, Y., Woodhead, J., Hellstrom, J., Wang, Y., Kong, X., and  
317 Spötl, C.: Improvements in  $^{230}\text{Th}$  dating,  $^{230}\text{Th}$  and  $^{234}\text{U}$  half-life values, and U–Th isotopic measurements by multi-  
318 collector inductively coupled plasma mass spectrometry, *Earth and Planetary Science Letters*, 371, 82–91, 2013.
- 319 Cullen, H., DeMenocal, P., Hemming, S., Hemming, G., Brown, F., Guilderson, T. and Sirocko, F.: Climate change and the  
320 collapse of the Akkadian empire: Evidence from the deep sea, *Geology*, 28, 379–382, 2000.
- 321 Cuthbert, M.O., Baker, A., Jex, C.N., Graham, P.W., Treble, P.C.: Andersen, M.S., Acworth, R.I.: Drip water isotopes in  
322 semi-arid karst: implications for speleothem paleoclimatology, *Earth and Planetary Science Letters*, 395, 194–204,  
323 2014.
- 324 Dansgaard, W.: Stable isotopes in precipitation, *Tellus*, 16, 436–468, 1964.
- 325 De Boer, E.J., Hooghiemstra, H., Florens, F.B.V., Baider, C., Engels, S., Dakos, V., Blaauw, M., and Bennett, K.D.: Rapid  
326 succession of plant associations on the small ocean island of Mauritius at the onset of the Holocene, *Quaternary  
327 Science Reviews*, 68, 114-125, 2013.
- 328 De Boer, E.J., Tjallingii, R., Vélez, M.I., Rijdsdijk, K.F., Vlug, A., Reichert, G.J., Prendergast, A.L., Louw, P.G.B.D., Florens,  
329 F.B.V., and Baider, C.: Climate variability in the SW Indian Ocean from an 8000-yr long multi-proxy record in the  
330 Mauritian lowlands shows a middle to late Holocene shift from negative IOD-state to ENSO-state, *Quaternary  
331 Science Reviews*, 86, 175-189, 2014.
- 332 De Boer, E.J., Velez, M.I., Rijdsdijk, K.F., Louw, P.G.D., Vernimmen, T.J., Visser, P.M., Tjallingii, R., and Hooghiemstra,  
333 H.: A deadly cocktail: How a drought around 4200 cal. yr BP caused mass mortality events at the infamous ‘dodo  
334 swamp’ in Mauritius, *Holocene*, 25, 2015.
- 335 Denniston, R.F., Wyrwoll, K.H., Polyak, V.J., Brown, J.R., Asmerom, Y., Jr, A.D.W., Lapointe, Z., Ellerbroek, R.,  
336 Barthelmes, M., and Cleary, D.: A Stalagmite record of Holocene Indonesian–Australian summer monsoon  
337 variability from the Australian tropics, *Quaternary Science Reviews*, 78, 155-168, 2013.
- 338 Denniston, R. F., Ummenhofer, C. C., Wanamaker, A. D., Lachniet, M. S., Villarini, G., Asmerom, Y., Polyak, V. J.,  
339 Passaro, K. J., Cugley, J., Woods, D., and Humphreys, W. F.: Expansion and contraction of the Indo-Pacific  
340 tropical rain belt over the last three millennia, *Scientific Reports*, 6, 34485, 2016.
- 341 Dorale, J. A., González, L. A., Reagan, M. K., Pickett, D. A., Murrell, M. T., and Baker, R. G.: A high-resolution record of  
342 Holocene climate change in speleothem calcite from Cold Water Cave, northeast Iowa, *Science*, 258, 1626-1630,  
343 1992.
- 344 Dorale, J. A., and Liu, Z.: Limitations of Hendy test criteria in judging the paleoclimatic suitability of speleothems and the  
345 need for replication, *Journal of Cave and Karst Studies*, 71, 73-80, 2009.
- 346 Draxler, R. R., and Hess, G. D.: An overview of the HYSPLIT\_4 modelling system for trajectories, *Australian  
347 Meteorological Magazine*, 47, 295-308, 1998.
- 348 Drysdale, R., Zanchetta, G., Hellstrom, J., Maas, R., Fallick, A., Pickett, M., Cartwright, I., Piccini, L.: Late Holocene  
349 drought responsible for the collapse of Old World civilizations is recorded in an Italian cave flowstone, *Geology*, 34,  
350 101-104, 2006.
- 351 Edwards, R.L., Chen, J., and Wasserburg, G.:  $^{238}\text{U}$ -  $^{234}\text{U}$ -  $^{230}\text{Th}$ -  $^{232}\text{Th}$  systematics and the precise measurement of time over  
352 the past 500,000 years, *Earth and Planetary Science Letters*, 81, 175–192, 1987.
- 353 Finné, M., Holmgren, K., Sundqvist, H. S., Weiberg, E., and Lindblom, M.: Climate in the eastern Mediterranean, and  
354 adjacent regions, during the past 6000 years—A review, *Journal of Archaeological Science*, 38, 3153-3173, 2011.

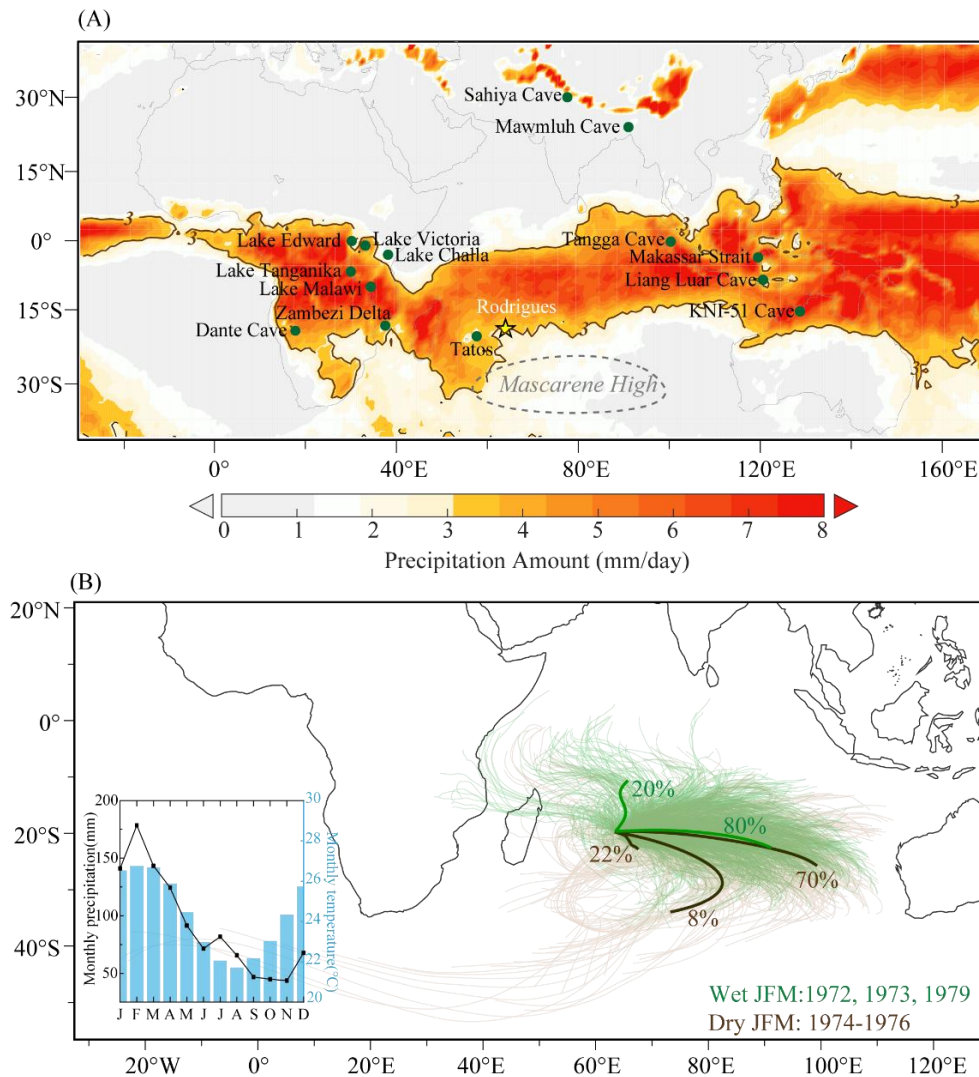


- 355 Fohlmeister, J.: A statistical approach to construct composite climate records of dated archives, *Quaternary Geochronology*,  
356 14, 48–56, 2012.
- 357 Freitas, A. C. V., Aímola, L., Ambrizzi, T., and de Oliveira, C. P.: Extreme Intertropical Convergence Zone shifts over  
358 Southern Maritime Continent, *Atmospheric Science Letters*, 18, 2-10, 2017.
- 359 Genty, D., Blamart, D., Ouahdi, R., Gilmour, M., Baker, A., Jouzel, J., and Van-Exter, S.: Precise dating of Dansgaard–  
360 Oeschger climate oscillations in western Europe from stalagmite data, *Nature*, 421, 833, 2003.
- 361 Griffiths, M.L., Drysdale, R.N., Gagan, M.K., Zhao, J.X., Ayliffe, L.K., Hellstrom, J.C., Hantoro, W.S., Frisia, S., Feng,  
362 Y.X., and Cartwright, I.: Increasing Australian-Indonesian monsoon rainfall linked to early Holocene sea-level rise,  
363 *Nature Geoscience*, 2, 636-639, 2009.
- 364 Griffiths, M. L., Kimbrough, A. K., Gagan, M. K., Drysdale, R. N., Cole, J. E., Johnson, K. R., Zhao, J. X., Cook, B. I.,  
365 Hellstrom, J. C., and Hantoro, W. S.: Western Pacific hydroclimate linked to global climate variability over the past  
366 two millennia, *Nature Communications*, 7, 11719, 2016.
- 367 Hendy, C. H.: The isotopic geochemistry of speleothems—I. The calculation of the effects of different modes of formation  
368 on the isotopic composition of speleothems and their applicability as palaeoclimatic indicators, *Geochimica et*  
369 *Cosmochimica Acta*, 35, 801-824, 1971.
- 370 Hong, Y. T., Hong, B., Lin, Q. H., Zhu, Y. X., Shibata, Y., Hirota, M., Uchida, M. Leng, X. T., Jiang, H.B., Xu, H., Wang,  
371 H., and Yi, L.: Correlation between Indian Ocean summer monsoon and North Atlantic climate during the  
372 Holocene, *Earth and Planetary Science Letters*, 211, 371-380, 2003.
- 373 Hong, B., Uchida, M., Hong, Y., Peng, H., Kondo, M., and Ding, H.: The respective characteristics of millennial-scale  
374 changes of the India summer monsoon in the Holocene and the Last Glacial, *Palaeogeography, Palaeoclimatology,*  
375 *Palaeoecology*, 496, 155-165, 2018.
- 376 Jaffey, A. H., Flynn, K. F., Glendenin, L. E., Bentley, W. T., and Essling, A. M.: Precision measurement of half-lives and  
377 specific activities of <sup>235</sup>U and <sup>238</sup>U, *Physical Review C*, 4, 1889, 1971.
- 378 Kalnay, E., Kanamitsu, M., Kistler, R., Collins, W., Deaven, D., Gandin, L., Iredell, M., Saha, S., White, G., Woollen, J.,  
379 Zhu, Y., Chelliah, M., Ebisuzaki, W., Higgins, W., Janowiak, J., Mo, K.C., Ropelewski, C., Wang, J., Leetmaa, A.,  
380 Reynolds, R., Jenne, R. and Joseph, D.: The NCEP/NCAR 40-year reanalysis project, *Bulletin of the American*  
381 *Meteorological Society*, 77, 437-472, 1996.
- 382 Kathayat, G., Cheng, H., Sinha, A., Yi, L., Li, X., Zhang, H., Li, H., Ning, Y., and Edwards, R.L.: The Indian monsoon  
383 variability and civilization changes in the Indian subcontinent, *Science Advances*, 3, e1701296, 2017.
- 384 Kathayat, G., Cheng, H., Sinha, A., Berkelhammer, M., Zhang, H., Duan, P., Li, H., Li, X., Ning, Y., and Edwards, R. L.:  
385 Evaluating the timing and structure of the 4.2 ka BP event in the Indian Summer Monsoon domain from an  
386 annually-resolved speleothem record from northeast India, *Climate of the Past Discussion*, in review, 2018.
- 387 Konecky, B. L., Russell, J. M., Johnson, T. C., Brown, E. T., Berke, M. A., Werne, J. P., and Huang, Y.: Atmospheric  
388 circulation patterns during late Pleistocene climate changes at Lake Malawi, Africa, *Earth and Planetary Science*  
389 *Letters*, 312, 318-326, 2011.
- 390 Lachniet, M. S.: Climatic and environmental controls on speleothem oxygen-isotope values, *Quaternary Science*  
391 *Reviews*, 28, 412-432, 2009.
- 392 Lashkari, H., Mohammadi, Z., and Keikhosravi, G.: Annual Fluctuations and Displacements of Inter Tropical Convergence  
393 Zone (ITCZ) within the Range of Atlantic Ocean-India, *Open Journal of Ecology*, 7, 12, 2017.
- 394 Marchant, R., and Hooghiemstra, H.: Rapid environmental change in African and South American tropics around 4000 years  
395 before present: a review, *Earth-Science Reviews*, 66, 217-260, 2004.
- 396 Markowska, M., Baker, A., Andersen, M.S., Jex, C.N., Cuthbert, M.O., Rau, G.C., Graham, P.W., Rutledge, H., Mariethoz,  
397 G., Marjo, C.E., Treble, P.C., Edwards, N.: Semiarid zone caves: evaporation and hydrological controls on  $\delta^{18}\text{O}$   
398 drip water composition and implications for speleothem paleoclimate reconstructions, *Quaternary Science Reviews*,  
399 131, 285–301, 2016.
- 400 Mayewski, P.A., Rohling, E.J., Stager, J.C., Karlén, W., Maasch, K.A., Meeker, L.D., Meyerson, E.A., Gasse, F., Van  
401 Kreveld, S., Holmgren, K., Lee-Thorp, K., Rosqvist, G., Rack, F., Staubwasser, M., Schneider, R.R., and Steig, E.J.:  
402 Holocene climate variability, *Quaternary Research*, 62, 243-255, 2004.
- 403 McDermott, F.: Palaeo-climate reconstruction from stable isotope variations in speleothems: a review, *Quaternary Science*  
404 *Reviews*, 23, 901-918, 2004.
- 405 Middleton, G. J., and David A. B.: Rodrigues—An Indian Ocean Island calcarenite: its history, study and management,  
406 *Coastal Karst Landforms*, Springer, Dordrecht, 261-276, 2013.
- 407 Migowski, C., Stein, M., Prasad, S., Negendank, J. F., and Agnon, A.: Holocene climate variability and cultural evolution in  
408 the Near East from the Dead Sea sedimentary record, *Quaternary Research*, 66, 421-31, 2006.
- 409 Morioka, Y., Takaya, K., Behera, S. K., and Masumoto, Y.: Local SST impacts on the summertime Mascarene high  
410 variability, *Journal of Climate*, 28, 678-694, 2015.
- 411 Railsback, L.B., Akers, P.D., Wang, L., Holdridge, G.A., Voarintsoa, N.: Layer-bounding surfaces in stalagmites as keys to  
412 better paleoclimatological histories and chronologies, *International Journal of Speleology*, 42, 167–180, 2013.

- 413 Railsback, L.B., Liang, F., Brook, G.A., Voarintsoa, N.R.G., Sletten, H.R., Marais, E., Hardt, B., Cheng, H., and Edwards,  
414 R.L.: The timing, two-pulsed nature, and variable climatic expression of the 4.2 ka event: A review and new high-  
415 resolution stalagmite data from Namibia, *Quaternary Science Reviews*, 186, 78-90, 2018.
- 416 Rijdsdijk, K.F., Hume, J.P., Bunnik, F., Florens, F.B.V., Baider, C., Shapiro, B., Plicht, J.V.D., Janoo, A., Griffiths, O., and  
417 Ostende, L.W.V.D.H.: Mid-Holocene vertebrate bone Concentration-Lagerstätte on oceanic island Mauritius  
418 provides a window into the ecosystem of the dodo (*Raphus cucullatus*), *Quaternary Science Reviews*, 28, 14-24,  
419 2009.
- 420 Rijdsdijk, K.F., Zinke, J., Louw, D.P.G.B., Hume, J.P., Plicht, V.D.H., Hooghiemstra, H., Meijer, H.J.M., Vonhof, H.B.,  
421 Porch, N., and Florens, F.B.V.: Mid-Holocene (4200 yr BP) mass mortalities in Mauritius (Mascarenes): insular  
422 vertebrates resilient to climatic extremes but vulnerable to human impact, *Holocene*, 21, 1179-1194, 2011.
- 423 Russell, J.M., Johnson, T.C., and Talbot, M.R.: A 725 yr cycle in the climate of central Africa during the late Holocene,  
424 *Geology*, 31, 677-680, 2003.
- 425 Schefuß, E., Kuhlmann, H., Mollenhauer, G., Prange, M., and Pätzold, J.: Forcing of wet phases in southeast Africa over the  
426 past 17,000 years, *Nature*, 480, 509, 2011.
- 427 Scroxton, N., Burns, S. J., McGee, D., Hardt, B., Godfrey, L. R., Ranivoharimanana, L., and Faina, P.: Hemispherically in-  
428 phase precipitation variability over the last 1700 years in a Madagascar speleothem record, *Quaternary Science*  
429 *Reviews*, 164, 25-36, 2017.
- 430 Senapathi, D., Underwood, F., Black, E., Nicoll, M. A., and Norris, K.: Evidence for long-term regional changes in  
431 precipitation on the East Coast Mountains in Mauritius, *International Journal of Climatology*, 30, 1164-1177, 2010.
- 432 Spötl, C., and Vennemann, T. W.: Continuous-flow isotope ratio mass spectrometric analysis of carbonate minerals, *Rapid*  
433 *Communications in Mass Spectrometry*, 17, 1004-1006, 2003.
- 434 Spötl, C.: Long-term performance of the Gasbench isotope ratio mass spectrometry system for the stable isotope analysis of  
435 carbonate microsamples, *Rapid Communications in Mass Spectrometry*, 25, 1683-1685, 2011.
- 436 Stanley, J.-D., Krom, M.D., Cliff, R.A., and Woodward, J.C.: Short contribution: Nile flow failure at the end of the Old  
437 Kingdom, Egypt: strontium isotopic and petrologic evidence, *Gearchaeology*, 18, 395-402, 2003.
- 438 Staubwasser, M., Sirocko, F., Grootes, P., and Segl, M.: Climate change at the 4.2 ka BP termination of the Indus valley  
439 civilization and Holocene south Asian monsoon variability, *Geophysical Research Letters*, 30, 2003.
- 440 Thompson, L. G., Mosley-Thompson, E., Davis, M. E., Henderson, K. A., Brecher, H. H., Zagorodnov, V. S., Mashiotta, T.  
441 A., Lin, P., Mikhalenko, V. N., Hardy, D. R., and Beer, J.: Kilimanjaro ice core records: evidence of Holocene  
442 climate change in tropical Africa, *Science*, 298, 589-593, 2002.
- 443 Tierney, J.E., Russell, J.M., Huang, Y., Damsté, J.S.S., Hopmans, E.C., and Cohen, A.S.: Northern Hemisphere controls on  
444 tropical southeast African climate during the past 60,000 years, *Science*, 322, 252-255, 2008.
- 445 Tierney, J.E., Russell, J.M., Damsté, J.S.S., Huang, Y., and Verschuren, D.: Late Quaternary behavior of the East African  
446 monsoon and the importance of the Congo Air Boundary, *Quaternary Science Reviews*, 30, 798-807, 2011.
- 447 Tierney, J.E., Oppo, D. W., LeGrande, A. N., Huang, Y., Rosenthal, Y., and Linsley, B. K.: The influence of Indian Ocean  
448 atmospheric circulation on Warm Pool hydroclimate during the Holocene epoch, *Journal of Geophysical Research:*  
449 *Atmospheres*, 117. 2012.
- 450 Treble, P.C., Baker, A., Ayliffe, L.K., Cohen, T.J., Hellstrom, J.C., Gagan, M.K., Frisia, S., Drysdale, R.N., Griffiths, A.D.,  
451 and Borsato, A.: Hydroclimate of the Last Glacial Maximum and deglaciation in southern Australia's arid margin  
452 interpreted from speleothem records (23–15 ka), *Climate of the Past*, 13, 667–687, 2017.
- 453 Wang, Y., Cheng, H., Edwards, R. L., He, Y., Kong, X., An, Z., Wu, J. Kelly, M. J., Dykoski, C. A., and Li, X.: The  
454 Holocene Asian monsoon: links to solar changes and North Atlantic climate, *Science*, 308, 854-857, 2005.
- 455 Weiss, H., Courty, M.-A., Wetterstrom, W., Guichard, F., Senior, L., Meadow, R., and Curnow, A.: The genesis and collapse  
456 of third millennium north Mesopotamian civilization, *Science*, 261, 995–1004, 1993.
- 457 Weiss, H.: Global megadrought, societal collapse and resilience at 4.2-3.9 ka BP across the Mediterranean and west Asia,  
458 *PAGES*, 24, 62–63, 2016.
- 459 Wurtzel, J.B., Abram, N.J., Lewis, S.C., Bajo, P., Hellstrom, J.C., Troitzsch, U., and Heslop, D.: Tropical Indo-Pacific  
460 hydroclimate response to North Atlantic forcing during the last deglaciation as recorded by a speleothem from  
461 Sumatra, Indonesia, *Earth and Planetary Science Letters*, 492, 264-278, 2018.
- 462 Yan, H., Wei, W., Soon, W., An, Z., Zhou, W., Liu, Z., Wang, Y., and Carter, R. M.: Dynamics of the intertropical  
463 convergence zone over the western Pacific during the Little Ice Age, *Nature Geoscience*, 8, 315, 2015.
- 464 Yoshimura, K., Kanamitsu, M., Noone, D., and Oki, T.: Historical isotope simulation using reanalysis atmospheric  
465 data, *Journal of Geophysical Research: Atmospheres*, 113, 2008.
- 466 Zielhofer, C., Suchodoletz, H.V., Fletcher, W.J., Schneider, B., Dietze, E., Schlegel, M., Schepanski, K., Weninger, B.,  
467 Mischke, S., and Mikdad, A.: Millennial-scale fluctuations in Saharan dust supply across the decline of the African  
468 Humid Period, *Quaternary Science Reviews*, 171, 119-135, 2017.

472  
473

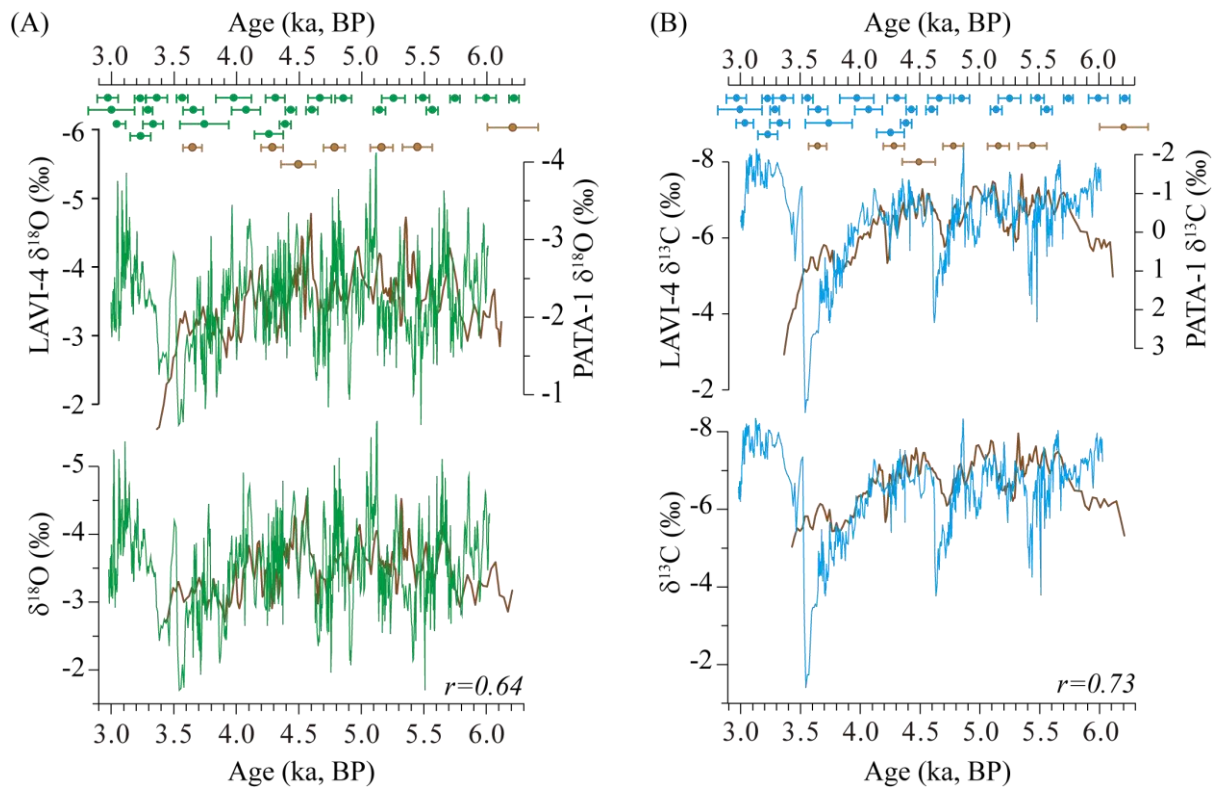
474 **Figures:**



475

476 **Figure 1.** Proxy locations and climatology. (A) Mean January to March (JFM) precipitation from the  
477 Tropical Rainfall Measuring Mission (TRMM) (<https://trmm.gsfc.nasa.gov/>) averaged over the period  
478 from 1997 to 2014. Shaded area bounded by solid brown lines (3 mm day<sup>-1</sup> isohyet) depict the mean  
479 position of the ITCZ. The dashed line shows the mean position of JFM 850 hPa geopotential height  
480 marking the location of the Mascarene High. Locations of Rodrigues Island (yellow star, this study) and  
481 other proxy sites (green dots) discussed in the text are also shown. (B) 4x daily low-level (~850 hPa)  
482 JFM air parcel back (120 hours) trajectory composites for anomalously wet (green) and dry (brown)  
483 years. Trajectories were computed using NOAA HYSPLIT model (Draxler and Hess, 1998) using  
484 NCEP/NCAR Reanalysis data (Kalnay et al., 1996). Bold lines indicate main cluster tracks associated  
485 with trajectories for wetter (green) and drier (brown) years. Inset shows mean monthly rainfall and  
486 temperature at Rodrigues averaged over the period 1951 to 2015.

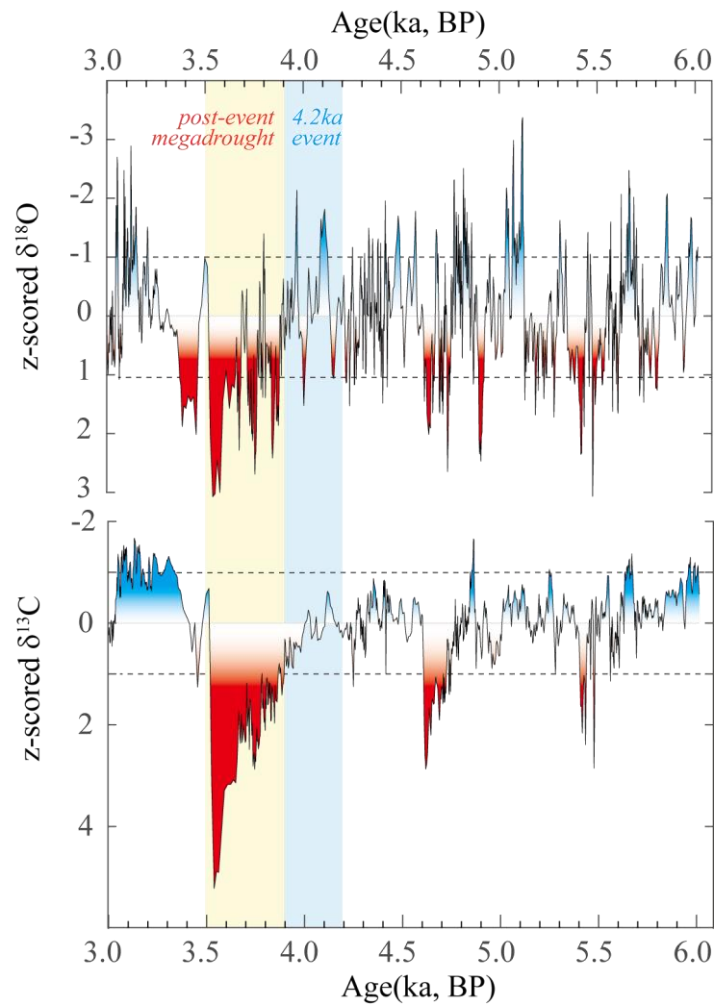
487



488

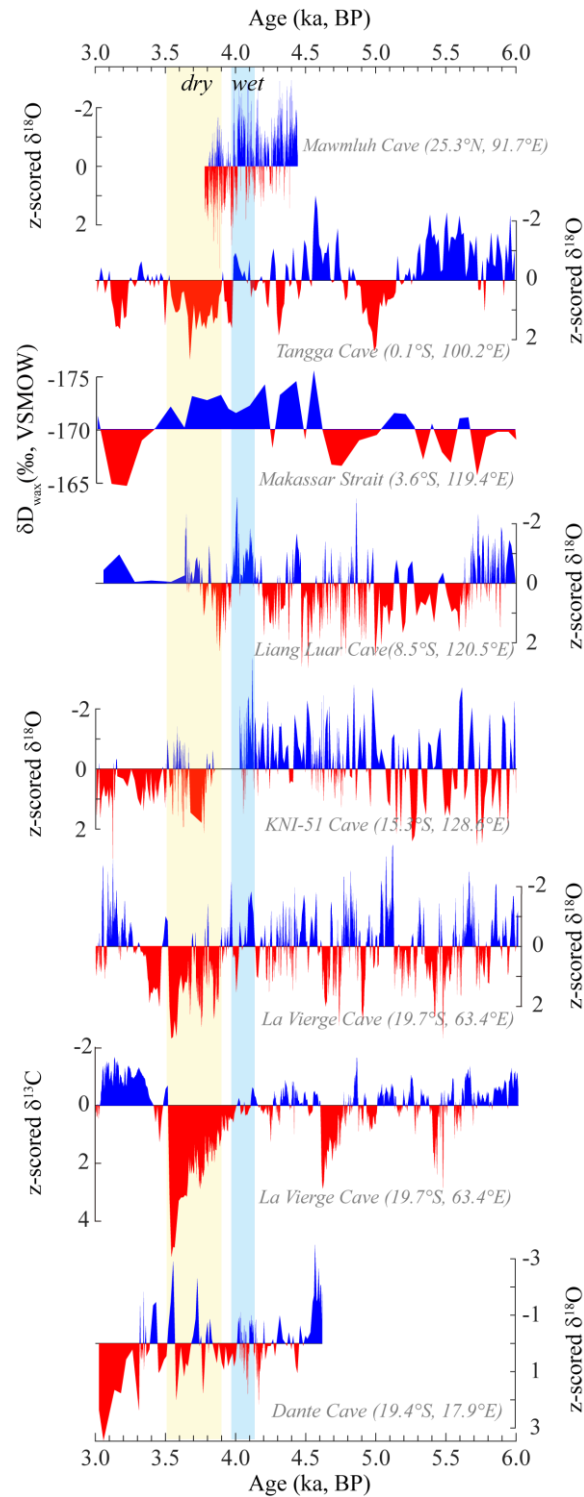
489

490 **Figure 2.  $\delta^{18}\text{O}$  and  $\delta^{13}\text{C}$  records of LAVI-4 and PATA-1.** (A)  $\delta^{18}\text{O}$  profiles of LAVI-4 (green) and  
 491 PATA-1 (brown) are shown on their independent COPRA age models (top) and ISCAM-derived age  
 492 models (bottom). The correlation coefficient ( $r$ ) between LAVI-4 and PATA-1 is 0.64. The PATA 1  
 493  $\delta^{18}\text{O}$  values were adjusted by  $\sim 1.3$  ‰ to match the LAVI-4 data series. (B) Same as in (A) but for the  
 494  $\delta^{13}\text{C}$  profiles of LAVI-4 and PATA-1. The PATA-1  $\delta^{13}\text{C}$  values were adjusted by  $\sim 6.5$  ‰ to match the  
 495 LAVI-4 values.



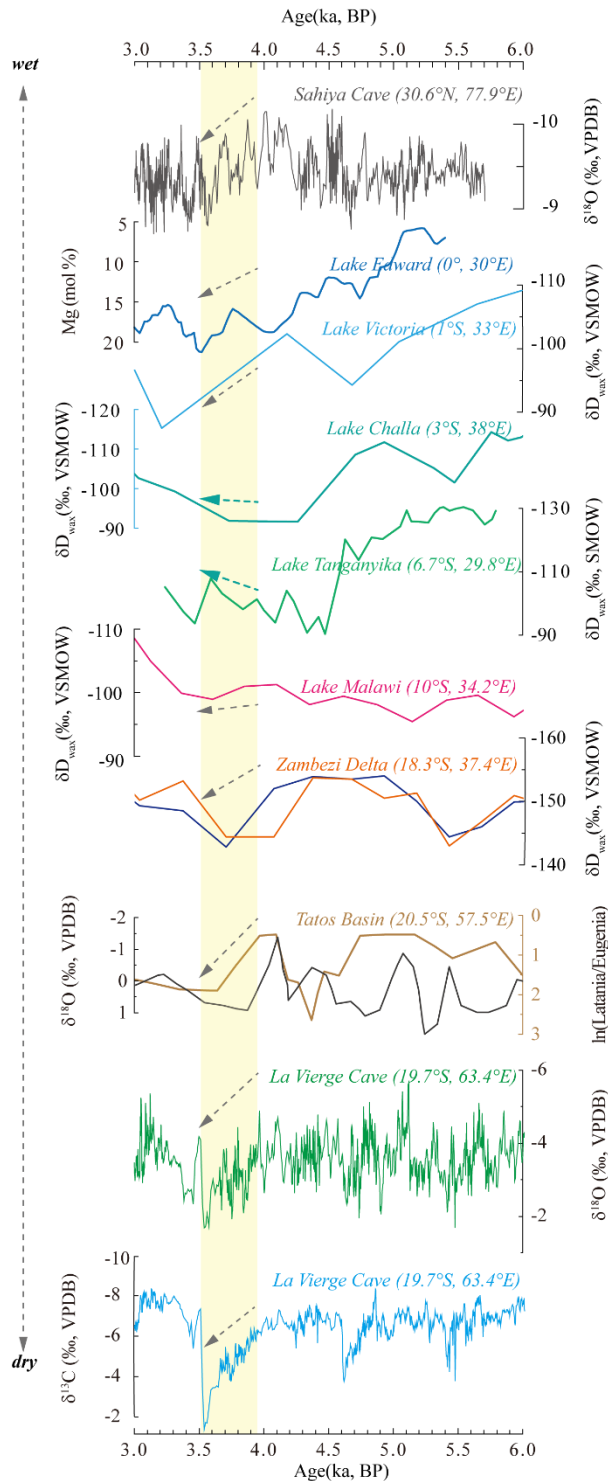
496

497 **Figure 3. Inferred hydroclimatic variability at Rodrigues from 6 to 3 ka BP.** LAVI-4  $\delta^{18}\text{O}$  and  $\delta^{13}\text{C}$   
 498 record are z-score transformed. Inferred droughts ( $z\text{-score} > 1$ ) and pluvial episodes ( $z\text{-score} < -1$ ) are  
 499 shaded (increasing saturation index indicates increasing intensity). Dashed lines indicate 1 standard  
 500 deviation. The blue bar marks the classical '4.2 ka event' interval and the yellow bar marks the 'post-  
 501 event', megadrought, inferred from LAVI-4.  
 502



503  
504  
505  
506  
507  
508  
509  
510  
511

**Figure 4. Comparison of LAVI 4 with climate proxy records from the eastern Indian Ocean.** From top to bottom, z-score transformed speleothem  $\delta^{18}\text{O}$  record from Mawmluh cave (Kathayat et al., 2018), Tangga cave, Sumatra, Indonesia (Wurtzel et al., 2018),  $\delta\text{D}_{\text{leaf wax}}$  record from marine sediment core BJ8-03-70GGC in the Makassar Strait (Tierney et al., 2012), z-score transformed speleothem  $\delta^{18}\text{O}$  records from Liang Luar cave, western Flores, Indonesia (Griffiths et al., 2009), KNI-51 cave, Kimberley, northwestern Australia (Denniston et al., 2013), La Vierge cave, Rodrigues (this study), and Dante cave, northeastern Namibia (Railsback et al., 2018). Shaded vertical bars mark periods of drier and wetter conditions.



512  
 513 **Figure 5. Comparison of LAVI-4 with climate proxy records from India and East Africa.** From top  
 514 to bottom:  $\delta^{18}\text{O}$  record from Sahiya cave, North India (Kathayat et al., 2017), Mg concentration of  
 515 endogenic calcite from Lake Edward (Russell et al., 2003),  $\delta\text{D}_{\text{leaf wax}}$  records from Lake Victoria (Berke  
 516 et al., 2012), Lake Challa (Tierney et al., 2011), Lake Tanganyika (Tierney et al., 2008), Lake Malawi  
 517 (Konecky et al., 2011),  $\delta\text{D}$  of n-C<sub>29</sub> alkanes (dark blue) and n-C<sub>31</sub> alkanes (orange) from the Zambezi  
 518 delta (Schefuß et al., 2011),  $\delta^{18}\text{O}$  record (black) and ln (Latania/Eugenia) records (brown) from Tatos  
 519 basin, Mauritius (De Boer et al., 2014), and the LAVI-4  $\delta^{18}\text{O}$  and  $\delta^{13}\text{C}$  record from La Vierge cave (this  
 520 study). The shaded vertical bar marks the megadrought from ~ 3.9 to 3.5 ka BP. Grey and green dashed  
 521 arrows mark the drying and wet trend inferred from East Africa lake records, respectively. All y axes  
 522 are inverted to show drier conditions down.  
 523